ScienSage

Journal of Advanced Scientific Research

Available online through http://www.sciensage.info

ISSN
0976-9595
Research Article

IRIDIUM (III) COMPLEXES OF 1-ALKYL -2-{(*O*-THIOALKYL) PHENYLAZO} IMIDAZOLES: SYNTHESIS, CHARACTERIZATION, DNA BINDING STUDY AND DFT CALCULATION

Dibakar Sardar

Department of Chemistry, Dinabandhu Andrews College, Garia, Kolkata, West Bengal, India

**Corresponding author: dibakardac@gmail.com*

ABSTRACT

The Ir(III) complexes of 1-Alkyl-2-{(*o*-thioalkyl)phenylazo}imidazole (SRaaiNR′, **1;** R = Me, R′ = Et (**a**); R = Et, R′ = Me (**b**); R = R′ = Et (**c**)), $[Ir(SRaaiNR')(PPh_3)Cl_2](ClO_4)$ (**2**) have been synthesized and characterized by elemental, mass and other spectral (IR, UV-Vis, and ^1H NMR) analysis. Based on several spectral analysis octahedral geometry has been proposed for the Ir(III) complexes. The DNA binding ability of the complexes (binding constant: 2.49 x 10^4 to 4.51 x 10^4) has been studied by absorption and fluorescence spectroscopic measurements. Density functional theory (DFT) computation technique on the optimized geometry of the complexes has been performed to interpret the electronic structures and their spectral properties.

Keywords: 1-Alkyl-2-{(*o*-thioalkyl) phenylazo}imidazoles, Ir(III) complexes, DNA binding study, DFT calculation

1. INTRODUCTION

The study of interaction between the transition metal complexes and DNA molecules plays extensive role in the development of anticancer drugs [1-4]. In the design of anticancer agents, metal complexes provide wide range due to the large diversity in structure, binding modes, and flexible ligand exchange kinetics [5]. The interaction of metal complexes with DNA forms the metal-DNA adducts which hampers DNA replication and ultimately results in the cell death [6].

The era of inorganic medicines in the field of chemotherapy research had started its journey with the discovery of anticancer activity of cisplatin and now inorganic medicines mainly platinum based drugs plays indispensable role in chemotherapy research [7]. In spite of the huge success, rapid development of drug resistance, adverse side effects, lack of selectivity, and severe toxicity of platinum-based drugs have shifted the direction of investigation towards other metal complexes. Over the last few years, a tremendous effort has been dedicated to develop other metals-based drugs with improved clinical effectiveness, reduced toxicity and wide range of selectivity [8-10]. Specially, the ruthenium complexes have drawn strong attention for their low toxicity, variable oxidation states and favourable kinetic aspects [11-14]. Recently, iridium complexes have attracted much attention due their tunable chemical and biological properties [15].

In this article, we report the synthesis, characterization and DNA binding property of Ir(III) complexes of 1-Alkyl-2-{(*o*-thioalkyl) phenylazo}imidazoles. The DNA binding property of the complexes is established by absorption and fluorescence spectroscopic studies.

2. EXPERIMENTAL

2.1. Material and physical measurements

$IrCl_3.3H_2O$ was purchased from Arora Matthey Ltd., India. The solvents and other chemicals were obtained from E. Merck, India. The ligands, 1-Alkyl-2-{(*o*-thioalkyl) phenylazo}imidazoles (SRaaiNR', **1**) have been prepared by following the literature reported procedure [16]. The solvents were dried before use [17]. The solution spectral studies were carried out with spectroscopic grade solvents.

Microanalyses (C,H, N) were carried out using Perkin-Elmer 2400 CHN elemental analyzer. Spectroscopic measurements were performed using the following instruments: ^1H NMR spectra in $CDCl_3$ (TMS as an internal standard), Bruker 300 MHz FT-NMR; The IR spectra, Perkin Elmer L120-00A FT IR

spectrophotometer (KBr disk); UV- Vis spectra, Lambda 25 Perkin Elmer;. Electrospray ionization (ESI) positive ion, mass spectra were recorded on a micro mass Q-TOF mass spectrometer. Molar conductance in 10^{-3} M solutions in acetonitrile was measured using a Systronics conductivity meter 304 model.

2.2. Synthesis

2.2.1. Synthesis of [Ir(SMeaaiNMe) (PPh_3)Cl_3] (ClO_4) (2a)

$IrCl_3.3H_20$ (182 mg, 0.517 mmol) was added to a methanol solution of 1-Methyl-2-{*o*-(thioethyl) phenylazo}imidazole (SMeaaiNEt) (128 mg, 0.517 mmol) and triphenylphosphine (136 mg, 0.517 mmol). The mixture was stirred and refluxed for 6 hours and cooled to room temperature. Then saturated aqueous solution of $NaClO_4$ was added which resulted a brown precipitate. The products were collected by filtration, washed with methanol and ether and dried under vacuum and was subjected to chromatography. A brown band was eluted with acetonitrile-toluene (1:3,v/v) which upon evaporation afforded analytically pure product **2a**. Yield was 284 mg (63%).

The other complexes were prepared by following the same procedure and the yields were 55-65%.

Anal. Calc. for [Ir(SMeaaiNEt) (PPh_3)Cl_2](ClO_4) (**2a**): C, 39.98; H, 3.10; N, 6.43. Found: C, 39.94; H, 3.06; N, 6.38%. UV (λ_{max}, nm (ε,M^{-1} cm^{-1}), CH_3CN): 592(2636), 489(9235), 425(14672), 280(19357). IR (KBr disk): $\nu_{N=N}$, 1379 cm^{-1}; $\nu_{C=N}$,1569 cm^{-1}; ν_{ClO4^-}, 1095 cm^{-1}; ν_{PPh3}, 519, 697, 751 cm^{-1}; ν_{Ir-Cl}, 297, 321.). TOF-MS: *m/z* 771 (M-ClO_4^-)$^+$, 735 (M-ClO_4^--Cl), 509 (M-ClO_4^-- PPh_3). ^{1}H-NMR (300 MHz, $CDCl_3$), δ (ppm): 1.45 (t, J = 7.5, 3H; N-R′:-CH_3), 2.88 (s, 3H; S-CH_3), 4.36 (q, J = 8.1 Hz, 3H; N-R′:-CH_2-), 7.14 (s, 1H; 5-H), 7.64(m, 2H; 9, 10-H), 7.79(s, 1H; 4-H), 8.02 (d, J = 7.6 Hz, 1H; 8-H), 8.28 (d, J = 7.5 Hz, 1H; 11-H), 7.26-7.50 (m, 15 H; PPh_3).

Anal. Calc. for [Ir(SEtaaiNMe) (PPh_3)Cl_2](ClO_4) (**2b**): C, 39.98; H, 3.10; N, 6.43. Found: C, 39.93; H, 3.02; N, 6.40%. UV (λ_{max}, nm (ε,M^{-1} cm^{-1}), CH_3CN): 592(2681), 491(9176), 423(14802), 282(19179). IR (KBr disk): $\nu_{N=N}$, 1367 cm^{-1}; $\nu_{C=N}$,1584 cm^{-1}; ν_{ClO4^-}, 1100 cm^{-1}; ν_{PPh3}, 522, 696, 750 cm^{-1}; ν_{Ir-Cl}, 305, 320. TOF-MS: *m/z* 771 (M-ClO_4^-)$^+$, 735 (M-ClO_4^--Cl), 509 (M-ClO_4^-- PPh_3). ^{1}H-NMR (300 MHz, $CDCl_3$), δ (ppm): 1.51 (t, J=8.1, 3H; S-R:-CH_3), 3.37(q, J=7.6, 3H; S-R:-CH_2-), 4.30(s, 3H; N-CH_3), 7.26(s, 1H; 5-H), 7.64 (m, 2H; 9, 10-H), 7.79 (s, 1H; 4-H), 8.08(d, J=7.0 Hz, 1H; 8-H), 8.29 (d, J=7.5 Hz, 1H; 11-H), 7.26-7.50 (m, 15 H; PPh_3).

Anal. Calc. for [Ir(SEtaaiNEt) (PPh_3)Cl_2](ClO_4) (**2c**): C, 39.34; H, 3.05; N, 6.33. Found: C, 39.28; H, 3.01; N, 6.27%. UV (λ_{max},nm (ε,M^{-1} cm^{-1}), CH_3CN): 591(2882), 488(9672), 422(15070), 277(20136). IR (KBr disk): $\nu_{N=N}$, 1369 cm^{-1}; $\nu_{C=N}$,1590 cm^{-1}; ν_{ClO4^-}, 1098 cm^{-1}; ν_{PPh3}, 523, 692, 754 cm^{-1}; ν_{Ir-Cl}, 306, 324. TOF-MS: *m/z* 785 (M-ClO_4^-)$^+$, 749 (M-ClO_4^- - Cl), 523 (M-ClO_4^-- PPh_3). ^{1}H-NMR ((300 MHz, $CDCl_3$), δ (ppm): 1.35 (t, J = 7.9, 3H; S-R:-CH_3), 1.57 (t, J =8.0, 3H; N-R′:-CH_3), 3.32(q, J =7.7, 3H; S-R:-CH_2-), 4.36(q, J = 8.3, 3H; N-R′:-CH_2-), 7.19 (s, 1H; 5-H), 7.59 (m, 2H; 9, 10-H), 7.85 (s, 1H; 4-H), 8.10(d, J = 7.6 Hz, 1H; 8-H), 8.35(d, J = 7.5 Hz, 1H; 11-H), 7.26-7.50 (m, 15 H; PPh_3).

2.3. Computational methods

All computations were performed using the Gaussian 09 program package [18]. All computations were performed at the level of the Becke's three-parameter hybrid exchange functional with nonlocal correlation functional of Lee-Yang-Parr (B3LYP) [19]. Elements except iridium were assigned a 6-31G basis set in our calculations. The Los Alamos effective core potential plus double zeta (LanL2DZ) [20] basis set were employed for iridium metal while 6-31G basis set were assigned for other elements. The geometric structure of the complex **2a** in the ground state (S_0) was fully optimized. The vibrational frequencies were calculated to ensure that optimized geometries represented local minima. Using the optimized S_0 geometry we employed time dependent density functional theory (TD-DFT) at the B3LYP level to predict the absorption characteristics [21].

2.4. DNA binding study

2.4.1. Preparation of the complex solution for DNA binding and nuclease studies

The stock solutions of complexes (2 mM) were prepared in acetone free methanol and diluted with Tris-HCl buffer to get required concentration before each set of experiments.

2.4.2. Preparation of calf thymus and pUC19 plasmid DNA

The solution of calf thymus (CT) DNA (Bangalore Genei, India) was prepared in 5 mM Tris-HCl / 50 mM NaCl buffer, pH 7.2 using deionised and sonicated

HPLC grade water. The CT-DNA used in the experiments was sufficiently free from protein (UV absorption ratio A_{260nm}/ A_{280nm} ~1.9). The DNA concentration was determined with the help of it extinction coefficient, ε of 6600 M^{-1} cm^{-1} at 260 nm. The DNA stock solution was stored at 4 °C and used within 4 days after preparation.

2.4.3. Ethidium bromide (EB) stock solution preparation

Ethidium bromide (EB) dust (Sigma-Aldrich, USA) was dissolved in double distilled water at a concentration of 1 mM. Stored stocks (at 4°C in dark) were diluted freshly before each experiment.

2.4.4. Ethidium bromide (EB) stock solution preparation

Absorption spectroscopic studies were done on a spectrophotometer (Perkin Elmer, lambda-25), The interaction between the metal complexes and CTDNA was observed by adding increasing concentrations of CT DNA (2 μM to 20 μM) to a fixed concentration of complex (40 μM) and increasing concentrations of complex (2 μM to 20 μM) to fixed concentration of CT DNA (100μM). After each addition, the DNA and complex mixtures were incubated at room temperature for 15 min and scanned from 250 nm to 700 nm. The self-absorption of DNA was eliminated in each set of experiments. Each sample was scanned for a cycle number of 2, cycle time of 5 sec at a scan speed of 100 nm/min. Modified Benesi-Hildebrand [22] plot was used for the determination of ground state binding constant between the complexes and CT DNA. The binding constant "K" was determined by using the following relation:

$$A_0/\Delta A = A_0/\Delta A_{max} + (A_0/\Delta A_{max}) \text{ X } 1/K \text{ X } 1/L_t$$

where $\Delta A = A_0 - A$, ΔA_{max} = maximum change in reduced absorbance,

A_0 = maximum absorbance of receptor molecules (without any ligand),

A = reduced absorbances of the receptor molecules (in presence of ligand),

L_t = ligand concentration.

2.4.5. Fluorescence spectroscopic studies of the complexes with EB bound DNA

Fluorescence spectroscopic studies of EB bound CT DNA with varying concentrations of the complexes (0-100μM) were done by using by LS 55 Perkin Elmer spectrofluorimeter at room temperature (298 K). The EB bound CT DNA was prepared fresh before each experiment by treating with 10^{-5} M DNA solution with 10^{-5} M EB solution and it was incubated for 30 min. The experiments were carried out with gradual addition of the complexes (10 μM) into EB bound DNA mixture, incubated for 15 min and the fluorescence spectra were taken. The excitation wavelength was 500 nm and the emission spectra were scanned from 510 nm to 750 nm.

The study is based on the competitive binding of the complex to DNA by replacing EB from EB bound DNA and this is observed by the quenching of the fluorescence intensity. The fluorescence quenching of EB bound DNA is expressed by the Stern-Volmer equation [23, 24]:

$$I_0/I = 1 + K_{SV}[Q] = 1 + kq\tau_0[Q]$$

where I_0 and I are the fluorescence intensities of BSA in the absence and in the presence of the quencher (i.e. the metal complex), respectively, K_{SV} is the Stern-Volmer quenching constant, [Q] is the concentration of the quencher, kq is the quenching rate constant of the biomolecule and τ_0 is the average lifetime of the molecule in the absence of the quencher.

A linear I_0/I *vs.* [Q] plot indicates that a single type of quenching mechanism is involved, either static or dynamic, while a deviation from linearity suggests a mixed quenching mechanism [25].

3. RESULTS AND DISCUSSION

3.1. Synthesis and formulation

The ligands, 1-Alkyl-2-{(*o*-thioalkyl)phenylazo} imidazoles (SRaaiNR′, **2;** (**a**); R = Me, R′ = Et (**a**); R = Et, R′ = Me (**b**); R = R′ = Et (**c**)) usually act as tridentate chelating ligands. The donor centres are imidazole-N (N), azo-N (N′) and thioaklyl(SR)-S (Scheme 1). The reaction of $IrCl_3$ with the ligand SRaaiNR′ (1) in the presence of triphenyl phisphine (PPh_3) in ethanol under stirring and refluxing condition afforded a red solution which upon addition of a saturated aqueous solution of $NaClO_4$ (Scheme 1) separated a red precipitate of composition, $[Ir(SRaaiNR')(PPh_3)Cl_2](ClO_4)$ (**2**). The compositions have been supported by elemental analysis and ESI (Positive ion) mass spectra. The complexes are diamagnetic in nature which confirms +3 oxidation state (d^6) for iridium. The conductance measurements in acetonitrile (Λ_M, 120–130 Ω^{-1} cm^2 mol^{-1}) propose 1:1 electrolyte nature of the complexes. $[Ir(SRaaiNR')(PPh_3)Cl_2]^+$ may exist in two octahedral isomeric forms

(**Scheme:1**); *cis*-MCl_2 type configuration, *i.e.* two chlorines are cis *w.r.t.* each other and *trans*-MCl_2 type configuration i.e. two chlorines are trans *w.r.t.* each other.

Because of unavailability of good quality crystals of **2** the spectral (UV-VIS, IR, ^{1}H-NMR, and Mass) techniques have been used to characterize the structure of the compounds. The spectral characterization shows that the configuration of the isolated complex **2** is *cis*-MCl_2 type.

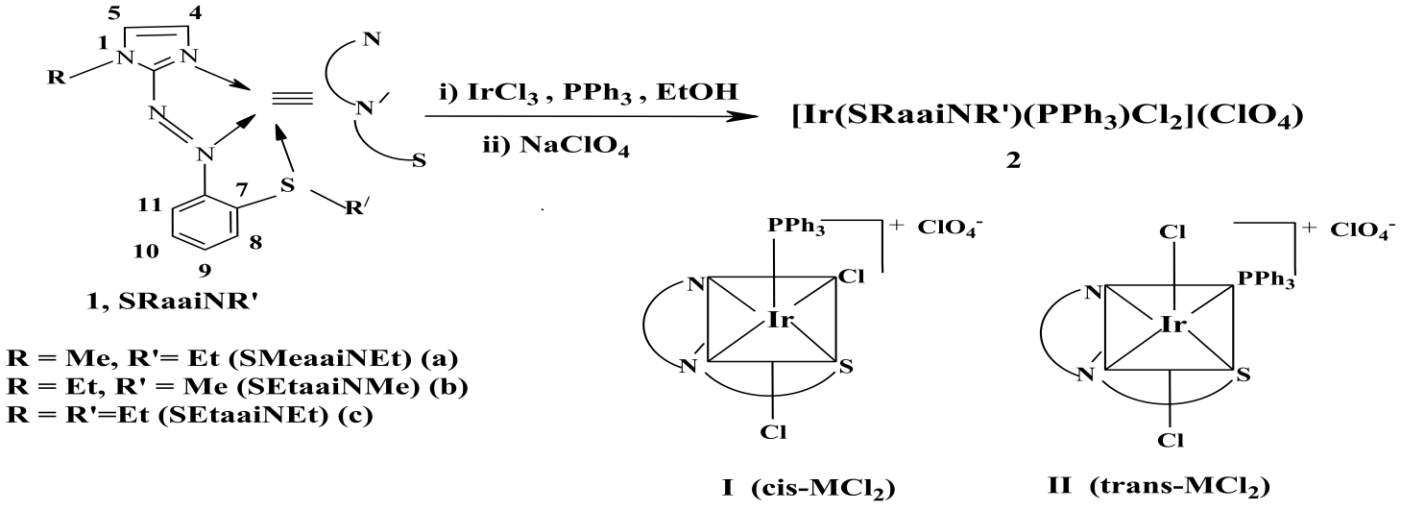

Scheme -1: The ligands and the complexes

3.2. Spectral characterization

The FT-IR spectra of the complexes recorded two $\nu_{Rh\text{-}Cl}$ stretches within the range 300-325cm^{-1} (**Fig.1**). This suggests the *cis*-MCl_2 type configuration for the complexes. The stretching frequencies for azo ($\nu_{N=N}$) appear at 1367-1379 cm^{-1} and imine ($\nu_{C=N}$) appear at 1579-1590 cm^{-1} and these stretching frequencies are significantly shifted to lower frequency compared to free ligand value ($\nu_{N=N,}$ 1400-1410 cm^{-1} and $\nu_{C=N,}$ 1600-1610 cm^{-1}) [16]. The appearance of these frequencies at lower values confirms the coordination of ligand to the metal centre through azo-N and imine-N. The presence of ClO_4^- as a counter ion is established by a strong and broad peak at 1090–1100 cm^{-1}, and a weak stretch around 620 cm^{-1}. The spectra also show three characteristics strong bands around 750, 695 and 525 cm^{-1} for coordinated PPh_3 ligand.

The mass spectra (ESI, Positive ion) of the complexes recorded expected fragmentation pattern with (M-ClO_4)$^+$ ion peak as base peak. The spectra of the complexes also recorded (M-ClO_4-Cl)$^+$ and (M-ClO_4-PPh_3)$^+$ ion peaks at expected values (**Fig.2**).

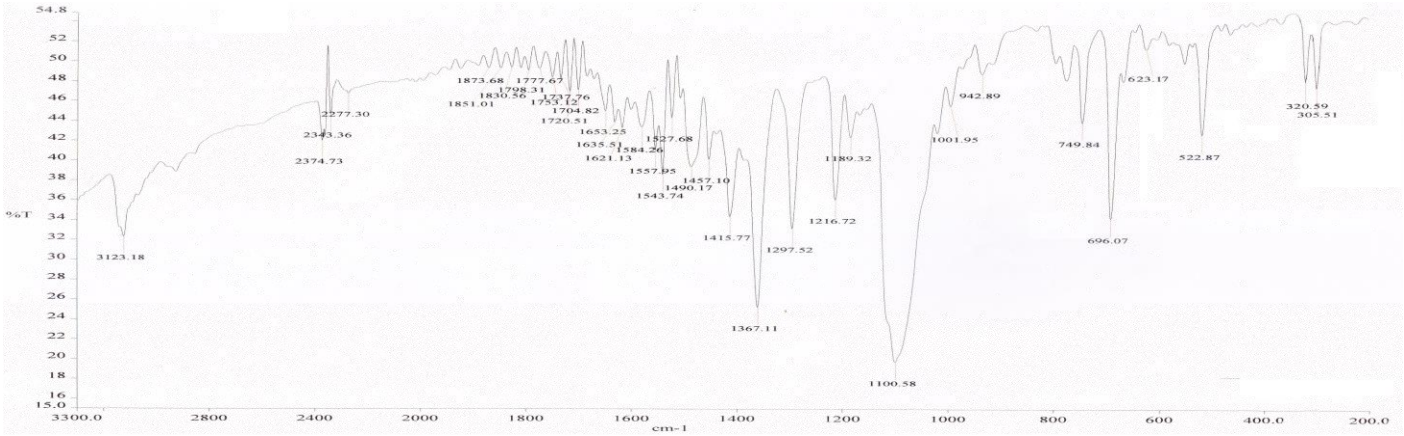

Fig.1: IR spectrum of 2b

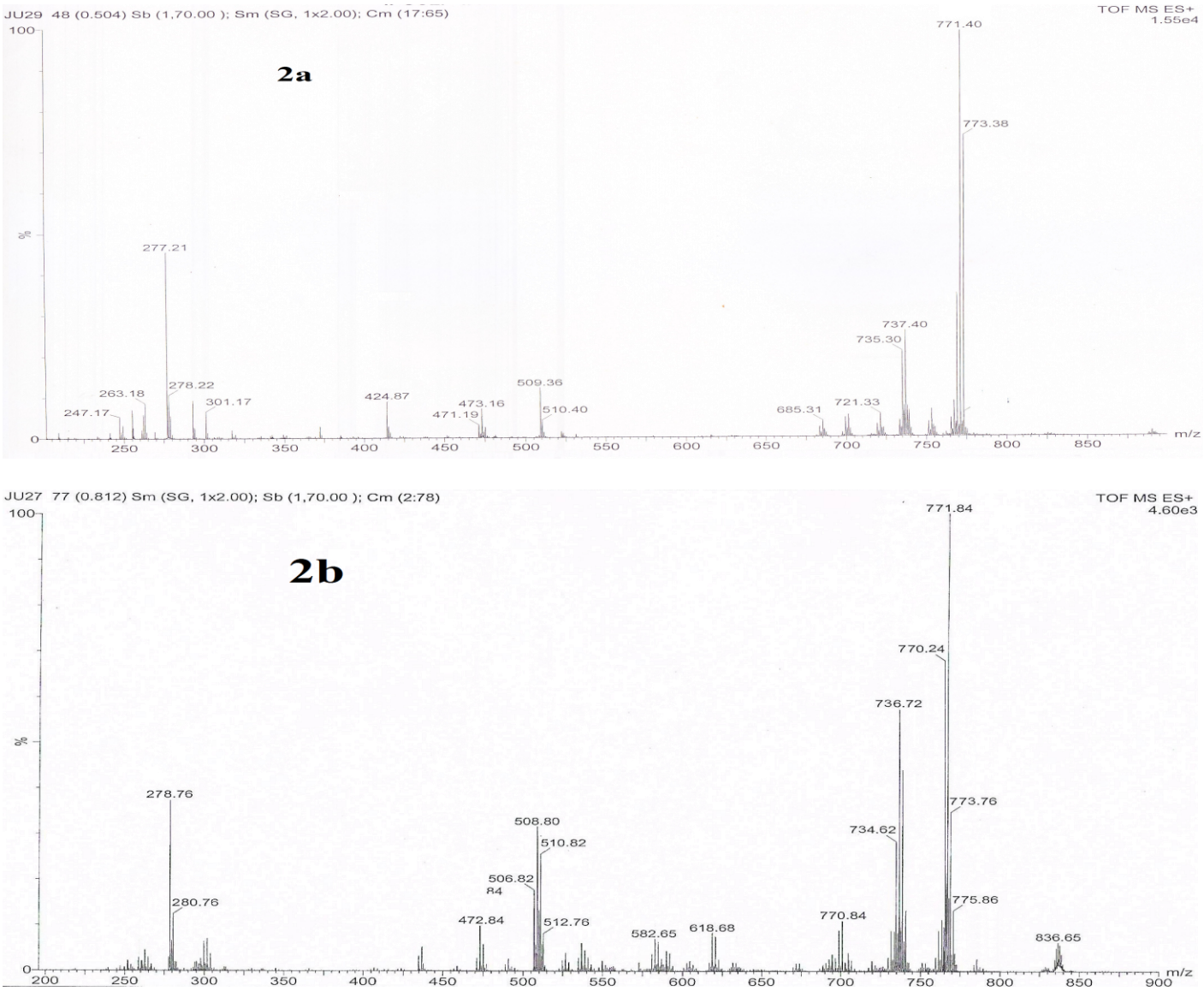

Fig.2: ESI(Positive ion) mass spectra of 2a and 2b.

The ^{1}H-NMR spectra of the complexes in $CDCl_3$ shows the downfield shifting of proton signals compared to free ligand data [16] which establishes the electron-withdrawing effect of the coordinated iridium (III). The imidazole proton, 4-H appears as a broad singlet at ~7.6-7.8 ppm with downfield shifting by 0.6-0.7 ppm and while 5-H appears at ~7.15-7.25 ppm with downfield shifting by ~0.2-0.3 ppm. These observations support the coordination of imine-N to the iridium centre. The '–CH_3' protons of 'SMe' group and '–CH_2-' protons of 'SEt' group suffer downfield shifting by 0.25-0.40 ppm compared to the free ligand position and appear as a singlet at around 2.90 ppm and quartet at 3.35 ppm respectively which supports the coordination of S of thioalkyl group (SR) to the metal centre. The resonances of the phenyl protons of triphenyl phosphine were observed in the region 7.20-7.50 ppm.

The absorption spectra of the complexes were investigated in acetonitrile solution (**Fig.3**). The red color solutions of the complexes show several intense absorptions in the visible and ultraviolet region. All the complexes show one high intense transitions ($\varepsilon \sim 10^4$ $M^{-1}cm^{-1}$) at ~425 nm along with a shoulder at ~490 nm($\varepsilon \sim 10^3$ $M^{-1}cm^{-1}$) and one weak transitions($\varepsilon \sim 10^2$ $M^{-1}cm^{-1}$) at ~600 nm in the visible region and one high intense transition ($\varepsilon \sim 10^4$ $M^{-1}cm^{-1}$) at ~285 nm in the UV region. The transitions in the visible region (> 400 nm) may be assigned as metal-to-ligand charge transfer transitions as these are not present in free ligands while the high energy transitions in the ultraviolet region (<

400 nm) may be considered as ligand centred transitions.

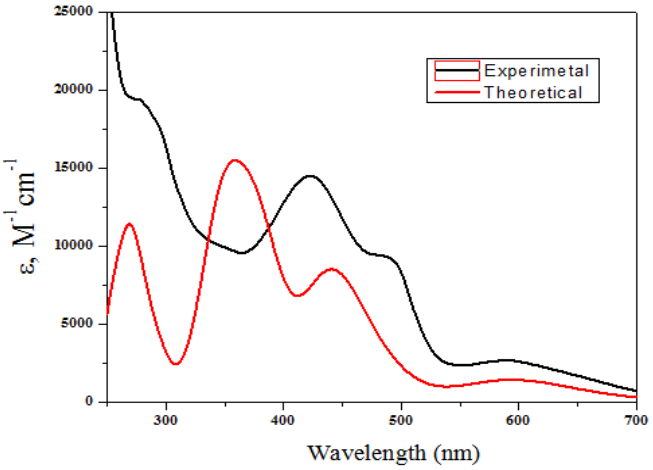

Fig. 3: Experimental and theoretical UV-Visible spectra of [Ir(SMeaaiNEt)(PPh_3)Cl_2](ClO_4)(2a)

3.3. DFT calculation and Electronic structure

Single crystal structure of the complexes could not be determined hence a theoretical structure of **2a** has been optimized in gas phase to get information about the structural parameters. The optimized structure is shown in **Fig.4** and relevant bond parameters are given in **Table 1**. These theoretical bond parameters show good agreement with the reported values. The figure showing that Iridium(III) is surrounded by two Cl (cis to each other), one P and N, N′, S donor centres of SMeaaiNEt forming a distorted-octahedral coordination environment. The ligand forms two adjacent five-membered chelate rings with chelate angles N(6)-Ir(68)-N(8), 77.55° and N(8)-Ir(68)-S(4), 86.03°. The *cis* chlorine angle, Cl(2)-Ir(68)-Cl(1) is 87.96°. The Ir-N(azo) length [Ir(65)-N(8), 2.001 Å] is shorter than the Ir-N(imidazole) lengths [Ir(65)-N(6), 2.065 Å] which may be due to better π-accepting ability of N(azo) centre.

The energies of highest occupied molecular orbital (HOMO) and lowest unoccupied molecular orbital (LUMO) are -7.71 eV and -6.67 eV respectively. HOMO is constituted by 39% of PPh_3, 34% of ligand and 27% of Cl. The LUMO is mostly delocalized on ligand π* orbitals (84%). The energy and the composition of some selected molecular orbitals are given in **Table 2** and surface plots of some frontier orbitals are shown in **Fig.5**.

To have a clear knowledge about the nature of electronic transitions the TD-DFT calculations were performed. The experimental spectra of **2a** correlate well with the theoretical spectra (**Fig.3**). The transition at around 585 nm is mainly due to the transitions from HOMO-3, HOMO-4 & HOMO → LUMO and can be regarded as admixture of chloride-to-ligand, (XLCT: Cl →Azo, Im) and metal-to-ligand (MLCT: Ir→Azo) charge transfer transitions (**Table 3**). The transitions in the region 400-500 nm are assigned to the mixture of multiple transitions originated due to intraligand charge transfer (ILCT) and PPh_3 to ligand charge transfer PPh_3 (YLCT). The other transitions at shorter wavelengths are mixture of mainly PPh_3-to-Metal (YMCT), intra-PPh_3 (IYCT), PPh_3-to-chloride (YXCT) charge transfer transitions.

Table 1: Selected theoretical bond lengths (Å) and angles (°) of 2a.

Bond length(Å)	Theoretical value	Bond angle (°)	Theoretical value
Ir(68)-N(6)	2.06453	N(6)-Ir(68)-N(8)	77.55
Ir(68)-N(8)	2.00122	N(8)-Ir(68)-S(4)	86.03564
Ir(68)-S(4)	2.37308	N(6)-Ir(68)-S(4)	163.48356
Ir(68)-Cl(1)	2.41158	N(8)-Ir(68)-Cl(2)	83.08657
Ir(68)-Cl (2)	2.46168	N(6)-Ir(68)-Cl(2)	84.69541
Ir(68)-P (3)	2.41529	S(4)-Ir(68)-Cl(1)	94.41069
N(7)-N(8)	1.28492	S(4)-Ir(68)-Cl(2)	91.63147
		P(3)-Ir(68)-Cl(2)	176.16873
		P(3)-Ir(68)-Cl(1)	91.47198
		P(3)-Ir(68)-N(6)	91.70635
		P(3)-Ir(68)-N(8)	97.44369
		P(3)-Ir(68)-S(8)	92.19048
		Cl(2)-Ir(68)-Cl(1)	87.96725

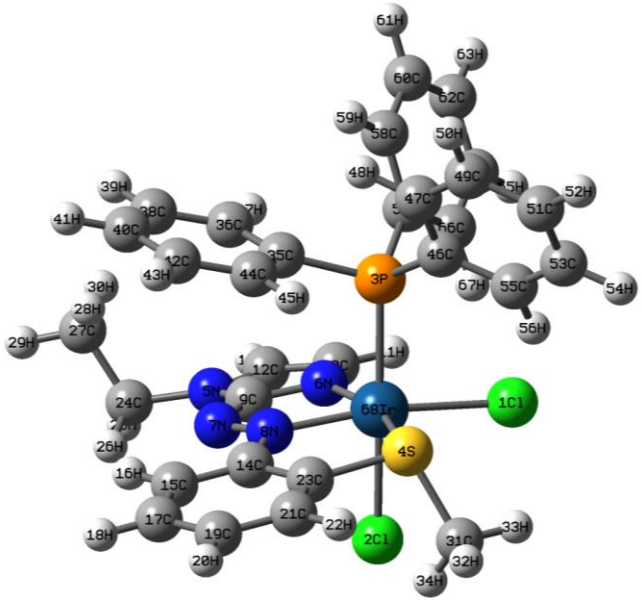

Fig.4: Optimised structure of [Ir(SMeaaiNEt) (PPh_3) Cl_2] (ClO_4)(2a)

Table 2: Selected orbital energies and percentage of orbital composition for [Ir(SMeaaiNEt)(PPh_3) Cl_2]ClO_4 (2a)

MOs		H-5	H-4	H-3	H-2	H-1	HOMO	LUMO	L+1	L+2	L+3	L+4	L+5
E(eV)		-9.24	-9.12	-8.46	-8.27	-7.9	-7.71	-6.67	-6.31	-6.16	-5.93	-5.44	-5.16
Ir		0	0	3	0	9	0	0	4	5	0	3	5
LIGAND	Azo	8	4	2	8	9	9	11	2	10	1	6	5
	Im	15	9	14	13	13	15	9	12	24	3	18	19
	Ph	17	06	02	11	13	5	30	0	10	81	14	26
	S-Me	21	5	21	17	9	5	34	28	7	10	24	06
Cl(1)		2	2	29	7	27	27	6	18	14	3	5	17
PPh_3		39	74	29	44	20	39	10	36	30	2	30	22

Note: Azo = -N=N- part, Im = Imidazole moiety, Ph = Phenyl moiety.

Table 3: Selected list of excited energies of [Ir(SMeaaiNEt) (PPh_3)Cl_2]ClO_4 (2a) obtained from TDDFT calculation in gas phase.

Excited State	λ, nm (Oscillator strength)	Transitions	Assignment
4	585 (0.014)	(55%) HOMO→LUMO (41%)HOMO-3→LUMO (11%)HOMO-4→LUMO	YLCT [PPh_3 →Azo, Im] ILCT [Im,Ph→ Azo,] XLCT [Cl →Azo, Im]
9	439 (0.096)	(49%)HOMO-8→LUMO (38%) HOMO-7→ LUMO	YLCT [PPh_3 →Azo, Im] ILCT [Im,Ph→Azo] XLCT [Cl →Azo, Im]
12	379 (0.1358)	(64%) HOMO-11→LUMO	ILCT [Im,Ph→Azo] YLCT [PPh_3 →Azo, Im] XLCT [Cl →Azo, Im]
14	353 (0.081)	(57%) HOMO-13→LUMO (19%)HOMO-12→LUMO (17%)HOMO→LUMO+1	ILCT [Im,Ph→Azo] MLCT [Ir→Azo] YLCT [PPh_3 →Azo, Im]
15	350 (0.058)	(54%) HOMO-12→ LUMO (18%)HOMO-14→LUMO (11%)HOMO-3→LUMO	YLCT [PPh_3 →Azo, Im] ILCT [Im,Ph→Azo] MLCT [Ir→Azo] XLCT [Cl →Azo, Im]
18	335 (0.019)	(39%)HOMO-14→LUMO (35%) HOMO-3→LUMO+1 (20%)HOMO-2→LUMO+1	ILCT [Im,Ph→Azo] LYCT [Cl → PPh_3] YMCT [PPh_3→Ir]
20	326 (0.0233)	(44%)HOMO-2→LUMO+2 (11%)HOMO-1→LUMO+1	ILCT [Im,Ph→Azo] LYCT [Cl → PPh_3] YMCT [PPh_3→Ir]
27	288 (0.088)	(67%)HOMO-4→LUMO+1	YLCT [PPh_3 → Azo, Im] IYCT [PPh_3 → PPh_3] YXCT [PPh_3 →Cl]
29	277 (0.023)	(54%) HOMO-6→LUMO+1	YLCT [PPh_3 → Azo, Im] IYCT [PPh_3 → PPh_3] YXCT [PPh_3 →Cl]
32	270 (0.0311)	(41%) HOMO-17→LUMO+1 (38%)HOMO-8→LUMO+1 (23%) HOMO-19→LUMO+1	ILCT [Im,Ph→Azo] LYCT [Cl → PPh_3] LXCT [Im,Ph →Cl]

38	262 (0.0172)	(52%)HOMO-4→LUMO+2 (12%)HOMO-3→LUMO+3	YLCT [PPh_3 → Azo, Im] IYCT [PPh_3 → PPh_3] YXCT [PPh_3 →Cl] YMCT [PPh_3 →Ir]
45	252 (0.0287)	(55%) HOMO-10→LUMO+1 (26%)HOMO-8→LUMO+2 (16%)HOMO-6→LUMO+2	YLCT [PPh_3 → Azo, Im] IYCT [PPh_3 → PPh_3] YXCT [PPh_3 →Cl]

Note: X = Cl, Y = PPh_3

ILCT = Intraligand charge transfer transition, MLCT = Metal to ligand charge transfer transition etc.

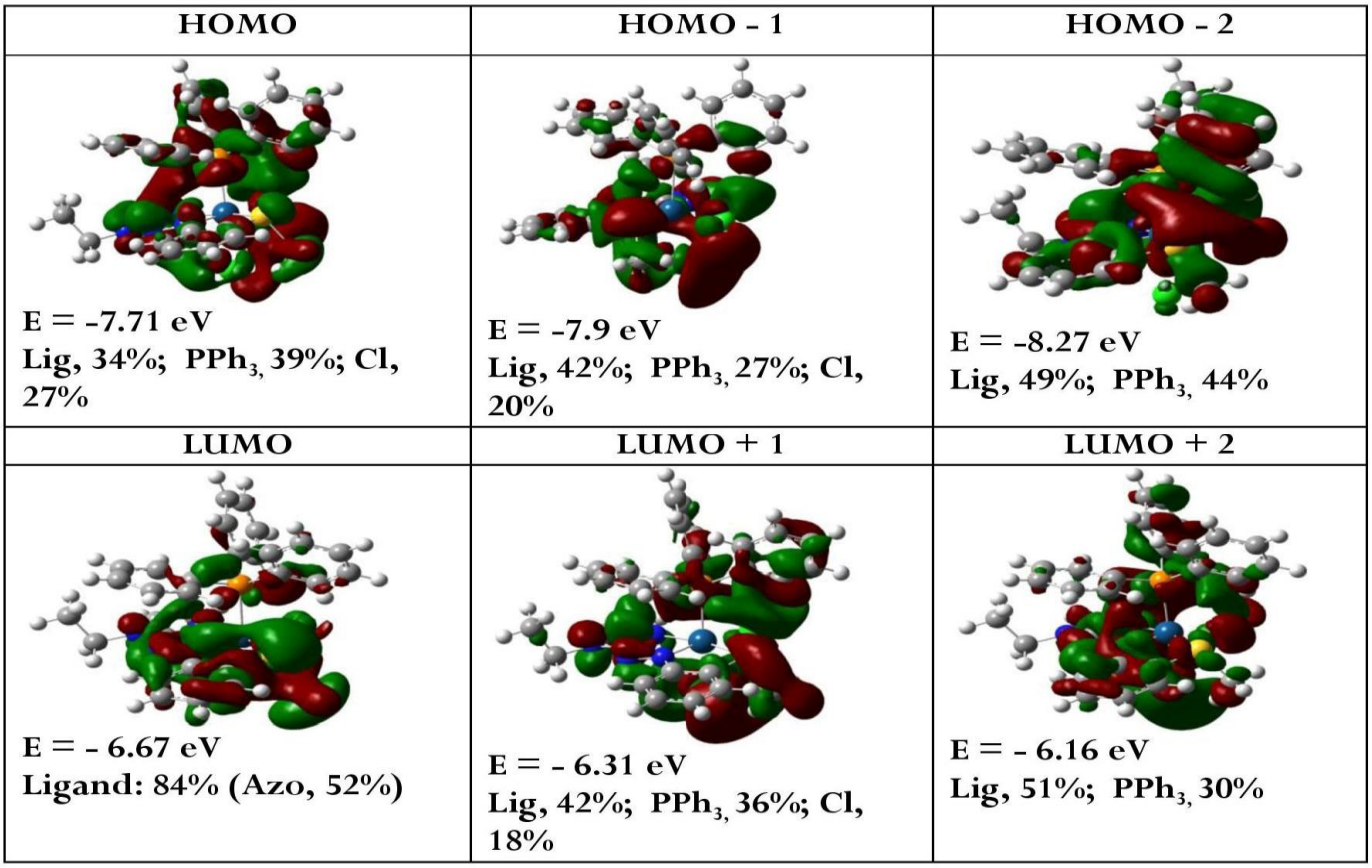

Fig. 5: Surface plots of some frontier orbitals of $[Ir(TaiEt)_2Cl_2]ClO_4$ (2b)

3.4. Interaction of complexes with DNA

3.4.1. Absorption spectroscopic studies of the complexes in presence of CT DNA

The interaction of the complexes with CT DNA was studied by observing the changes in UV-VIS absorption spectra because any kind of change in absorption spectra due to their mixing is the direct evidence of interaction between them [26]. Upon addition of increasing concentrations of complexes to fixed concentration of CT DNA (100μM), the absorption of DNA at 260nm was decreased gradually and the reverse course of action, *i.e.* addition of increasing concentrations of CT DNA to fixed concentration of complexes recorded a steady decrease in absorption with a slight red shift (**Fig. 6-7**). Such changes in absorbance clearly indicate existence of some specific interaction between the complex and DNA molecules. To compare the binding ability of the complexes, we have calculated the ground state binding constant(K_b) between the complexes and DNA at the absorption maximum of DNA by using modified Benesi-Hildebrand (BH) plot [22] (**Fig.6-7**) and the binding constants are 4.11 x 10^4 M^{-1} (**2a**), 4.51 x10^4 (**2b**) and 2.49 x 10^4 (**2c**). The observed binding constants (K_b) revealed that the complex **2a** binds strongly with CT DNA than the other complexes.

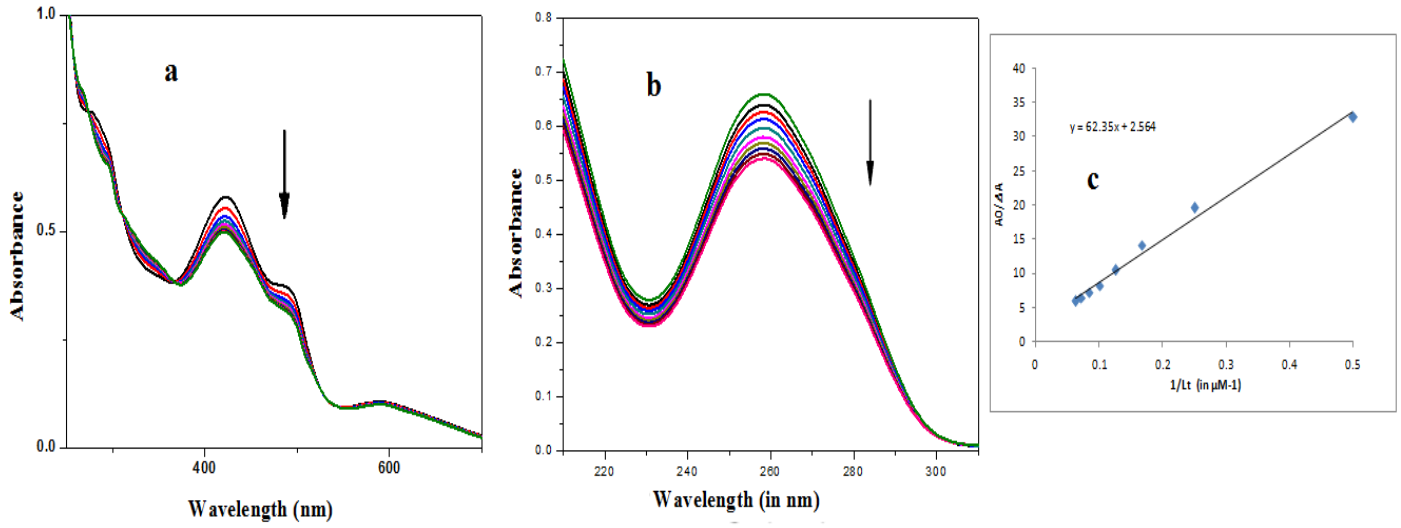

Fig. 6: (a) Absorption spectroscopic study of 40 μM complex 2a with increasing concentrations of CT DNA (0, 1, 2, 4, 6, 8, 10, 12, 14, 16, 18 and 20 μM) respectively. (b) Absorption spectroscopic study of CT DNA (100 μM) with increasing concentrations of complex 2a (0, 2, 4, 6, 8, 10, 12, 14, 16, 18 and 20 μM) respectively. (c) Modified Benesi-Hildebrand plot for the determination of ground state binding constant between CT DNA and the complex 2a.

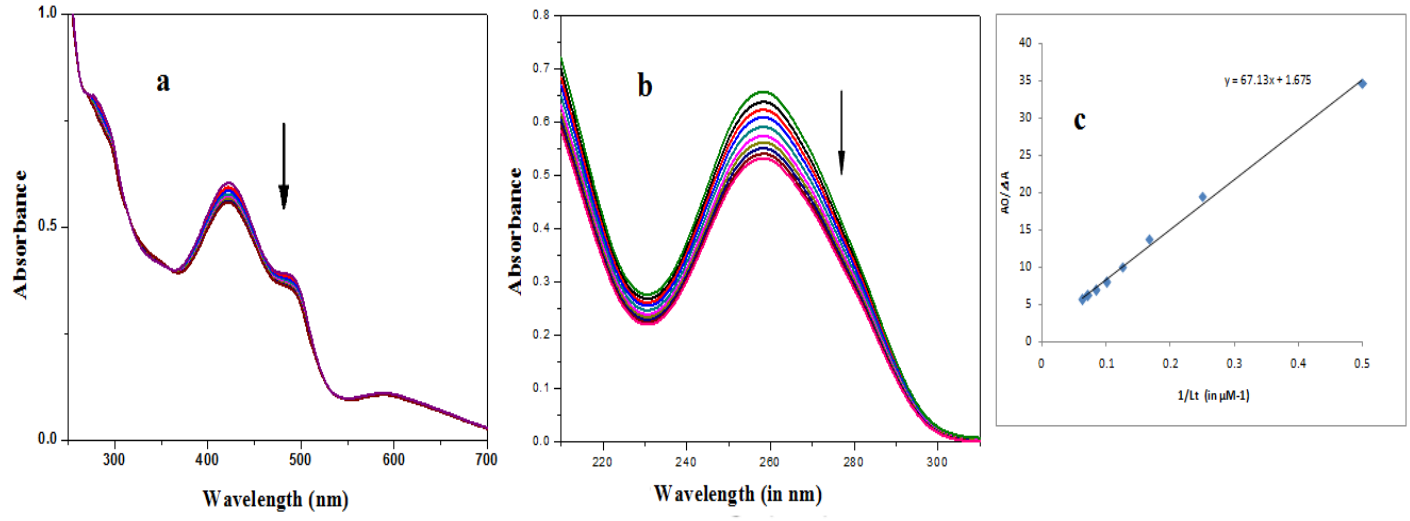

Fig. 7: (a) Absorption spectroscopic study of 40 μM complex 2c with increasing concentrations of CT DNA (0, 1, 2, 4, 6, 8, 10, 12, 14, 16, 18 and 20 μM) respectively. (b) Absorption spectroscopic study of CT DNA (100 μM) with increasing concentrations of complex 2c (0, 2, 4, 6, 8, 10, 12, 14, 16, 18 and 20 μM) respectively. (c) Modified Benesi-Hildebrand plot for the determination of ground state binding constant between CT DNA and the complex 2c.

3.4.2. Fluorescence spectroscopic studies of the complexes with ethidium bromide (EB) bound DNA

The interaction between DNA and complex molecules was further confirmed by studying the ability of the complexes to displace ethidium bromide (EB) from EB bound DNA. The DNA or EB molecules do not have fluorescence property alone but being a fluorescence probe in presence of DNA, EB releases intense fluorescent light due to its strong intercalation between adjacent base pairs. The fluorescence spectroscopic studies showed that the gradual increase of concentration of complexes to the EB bound DNA solution caused quenching in fluorescence intensity

which follow the linear Stern-Volmer equation (**Fig.9**). The Stern-Volmer quenching constants (K_{sv}) obtained from the slope of the plot [Q] versus I_0/I are $5.41x10^3M^{-1}$(**2a**), $6.632x10^3M^{-1}$(**2b**), and $4.936\ x10^3M^{-1}$(**2c**). The apparent binding constant (K_{app}) was also calculated from the equation $K_{EB}[EB] = K_{app}[complex]$, where $K_{EB} = 1.0x10^7\ M^{-1}$, [EB] = 50 μM, and [complex] is the concentration that causes a 50% quenching of the initial EB fluorescence [27]. The K_{app} values of the complexes are $2.79x10^5$ (**2a**), $3.36x10^5$ (**2b**) and $2.44x10^5$ (**2c**). The magnitudes of K_{sv} and K_{app} values of the complexes suggest that the interaction of complexes with DNA is strong [27].

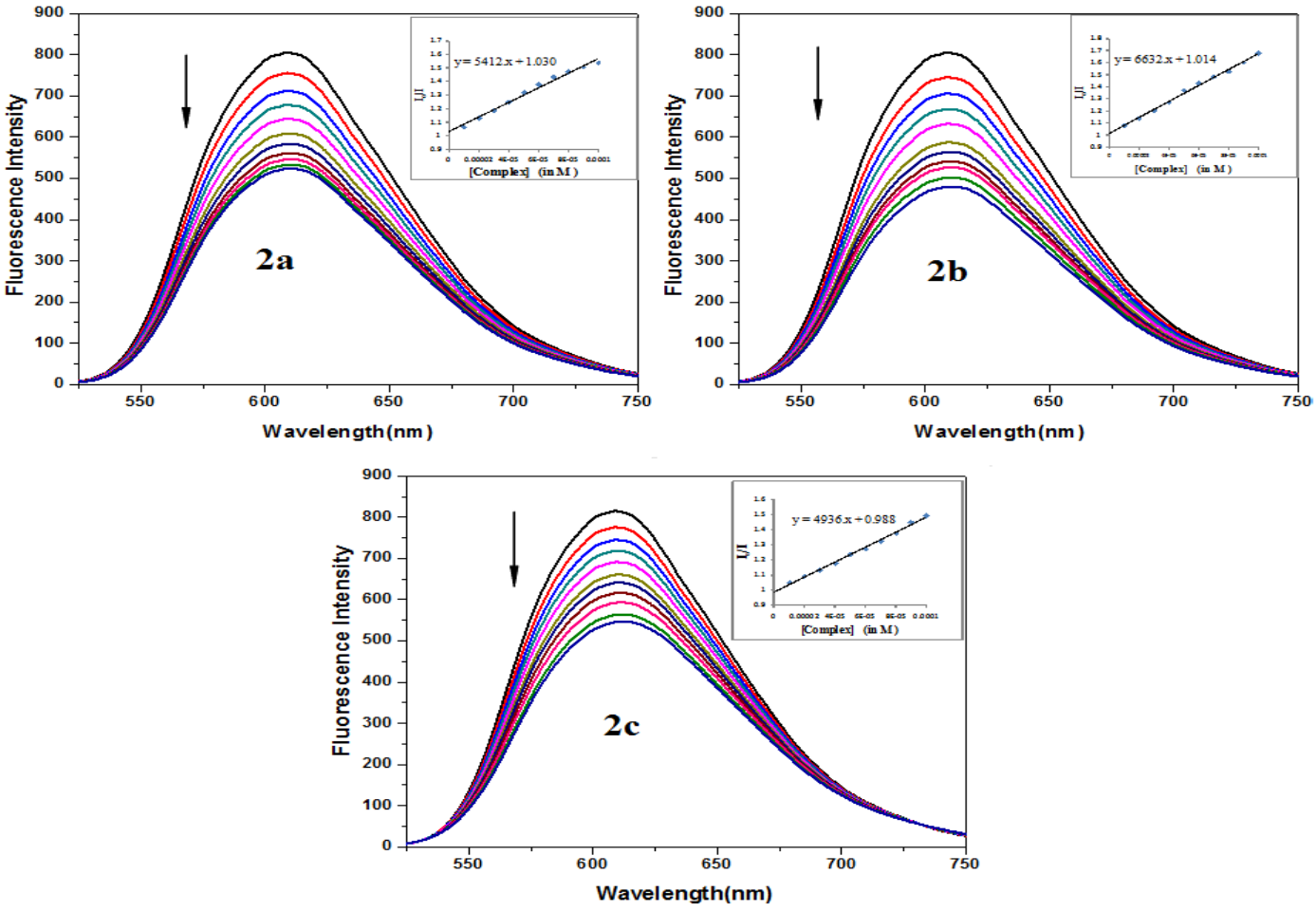

Fig. 8: Fluorescence spectroscopic study of EB bound DNA with increasing concentrations (0, 10, 20, 30 40, 50, 60, 70, 80, 90 and 100 μM) of 2a, 2b and 2c respectively. Inset picture shows Stern–Volmer plot for complexes.

4. CONCLUSION

The Ir(III) complexes of 1-Alkyl-2-{(*o*-thioalkyl) phenylazo}imidazole have been synthesized characterized by elemental and spectroscopic techniques. The spectral characterization suggests octahedral geometry with *cis*-MCl_2 type configuration for the Ir(III) complexes. Density functional theory (DFT) study interprets the electronic structures and their spectral properties. The DNA binding study by absorption and fluorescence spectroscopic methods show the DNA binding ability of the complexes. The complex **2b** binds most strongly while the least binding ability was observed in case of complex **2c**.

5. ACKNOWLEDGEMENTS

Author acknowledges Professor Chittaranjan Sinha, Professor, Department of Chemistry, Jadavpur University, for providing the research facilities and his valuable suggestions.

6. REFERENCES

1. Sun RW-Y, Ma D-L, Wong EL-M, Che C -M. *Dalton Trans.*, 2007; **43**:4884-4892.
2. Cutillas N, Yellol GS, de Haro C, Vicente C, Rodríguez V, Ruiz J. *Coord. Chem. Rev.,* 2013; **257:**2784-2797.
3. Heydari M, Moghadam ME, Tarlani A, Farhangian H. *Appl. Biochem. Biotech.,* 2017; **182(1):**110-127
4. Dehkhodaei M, Sahihi M, Rudbari HA, Gharaghani S, Azadbakht R, Taheri S, Kajani AA. *J. Mol. Liq.*, 2017; **248:** 24-35.
5. Gasser G, Ott I, Metzler-Nolte N. *J. Med. Chem.,* 2011; **54(1):**3-25.
6. Johnstone TC, Suntharalingam K, Lippard SJ. *Chem. Reviews*, 2016; **116(5):**3436-3486.
7. Mukhopadhyay S, Gupta RK, Paitandi RP, Rana NK, Sharma G, Koch B, Rana LK Hundal MS, Pandey DS. *Organometallics*, 2015; **34(18):**4491-4506.
8. Wang XL, Zheng K, Wang LY, Li YT, Wu ZY, Yan CW. *Appl. Organomet. Chem.,* 2016; **30(9):**730-739.
9. Mehta JV, Gajera SB and Patel MN. *Med. Chem. Com.,* 2016; **7(7):**1367-1380.
10. Li Y, Yang Z, Zhoua M, Li Y. *RSC Adv.*, 2017; **7:** 49404-49422.
11. Kostrhunova H, Florian J, Novakova O, Peacock AFA, Sadler PJ, Brabec V. *J. Med. Chem.,* 2008; **51:**3635-3643.
12. Aird RE, Cummings J, Ritchie AA, Muir M, Morris RE, Chen H, Sadler PJ, Jodrell DI. *Br. J. Cancer*, 2002; **86:**1652-1657.
13. Loughrey BT, Healy PC, Parsons PG, Williams ML. *Inorg. Chem.*, 2008; **47:**8589-8591.
14. Mendoza-Ferri MG, Hartinger CG, Mendoza MA, Groessl M, Egger AE, Eichinger RE, et al. *J. Med. Chem.,* 2009; **52:**916-925.
15. Ma D-L, Wu K-J, Leung C-H. *Molecules*, 2019; **24**:2739-2753.
16. Banerjee D, Ray U, Jasimuddin Sk, Liou J–C, Lu T–H, Sinha C. *Polyhedron,* 2006; **25:**1299-1306.
17. Vogel AI, Tatchell AR, Furnis BS, Hannaford AJ, Smith PWG. A Text Book of Practical Organic Chemistry, 5th Edn (Prentice Hall); 1996.
18. H. B. Schlegel et al. Gaussian 09, Revision A.02, Gaussian, Inc., Wallingford CT, 2009.
19. Lee C, Yang W, Parr RG. *Phys. Rev. B*, 1988; **37:**785-789.
20. Hay PJ, Wadt WR. *J. Chem. Phys.*, 1985; **82:**270-283.
21. EMSL, basis set library available http:/www.emsl.pnl.gov/forms/basisform.html
22. Benesi HA, Hildebrand JH. *J. Am. Chem. Soc.*, 1949; **71:**2703-2707.
23. J.R. Lakowicz. Principles of Fluorescence Spectroscopy. Second Edition ed. New York: Kluwer Academic/Plenum Publishers; 1999.
24. Valeur B. Molecular Fluorescence. Principles and Applications. Weinheim: Wiley; 2001.
25. Eftink MR, Ghiron CA. *Anal. Biochem.*, 1981; **114:**199-227.
26. Pyle AM, Rehmann JP, Meshoyrer R, Kumar CV, Turro NJ, Barton JK. *J. Am. Chem. Soc.,* 1989; **111:**3051-3058.
27. García-Giménez JL, González-Álvarez M, Liu-González M, Macías B , Borrás J, Alzuet G. *J. Inorg. Biochem.*, 2009; **103:**923-934.